CHAPTER III

MULTI STEPPED BEAM RECONFIGURATION IN PLANAR ANTENNA USING PIN DIODES

3.1 Introduction

Reconfiguration of beam patterns in antennas helps in reducing multipath propagation and the noise from the unwanted directions by pointing the beam towards the targeted user [1-5]. While steering the beam pattern, stability of return loss and sufficiently good gain at all the reconfigured beam directions needs to be maintained. Multi-stepped sweeping of the beam using a single radiating planar element is always challenging.

Conventionally, arrays, reflecting planes or parasitic elements are used for beam pattern reconfiguration [5-11]. In a microstrip design, parasitic elements of various forms are commonly used with planar radiators to steer the beam [12, 13]. The concept of Yagi-Uda antenna is employed to adaptively switch the beam [1, 14-16].

This chapter presents a scheme to sweep the beam in multiple steps. A planar rectangular microstrip patch (RMA) antenna is used as the driven element and is surrounded by four sets of parasitic elements. Each set of parasitic elements is further segmented into metallic strips. Each strip is activated/deactivated via a PIN diode. Beam steering of the RMA from its broadside direction is achieved by modifying the beam directing ability of the strips by switching on/off the PIN diode. The proposed prototype antenna is tested for its performance for various beam sweeping configurations.

3.2 Topology of beam scanning patch antenna

The proposed beam scanning antenna is an implementation of the Yagi antenna principle for a planar configuration. The antenna comprises of two basic parts, driven rectangular patch and parasitic elements, placed at the corners of the RMA.

3.2.1 Driving antenna

A rectangular patch is designed to resonate at 8.00 GHz using Transmission Line Model [17] on an FR4 substrate ($\varepsilon = 4.4$) of thickness 1.6 mm. The antenna is edge fed by a microstrip line and a quarter wave transformer. The calculated patch dimensions are $W = 11.52$ mm and $L = 8.38$ mm.

3.2.2 Directing elements

The parasitic elements are thin metallic strips placed in a co-planar configuration to the RMA. They are positioned at the four corners of the driven patch in a set of four strips. The purpose of the elements is to shift the beam of the RMA from the broadside direction, by acting as directing elements to the microstrip patch. The formation uses the Yagi design principle, where the length ratio between the director and the driven patch is important. The ratio should be in between 0.8 to 1 [18], otherwise, there will be negligible effect of the parasitic element on the beam pattern. Here, the overall length of each strip, S_L is kept equal to the length, L, of the driven patch. A schematic of the proposed antenna design is shown in Figure 3.1.

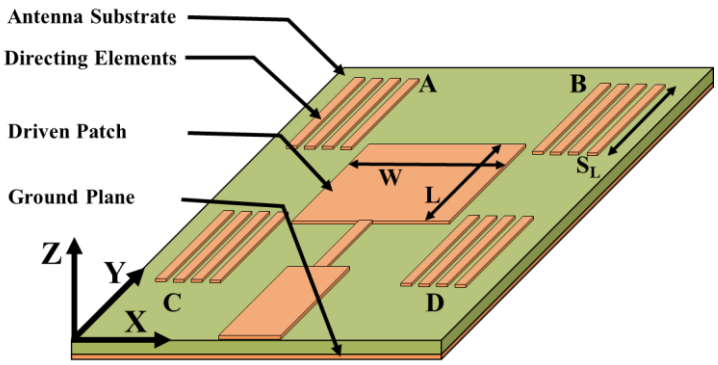

Figure 3.1 Schematic diagram of the proposed antenna. W = 11.52 mm, L = 8.38 mm and A, B, C, D represents the position of the parasitic

Performance of the beam steering antenna dependents on the relative positions of parasitic elements and the main radiator. To get the desired beam reconfigurability, consistent gain, directivity and stable return loss, the positions of the directing elements are optimized in CST MW studio.

3.2.3 Optimization of size, number and placement of the directing elements

From the simulation study it is observed that input impedance of the designed patch antenna is depended on the position of the directing strips. In order to obtain a better impedance matching, strips positions are optimized. The optimization process is carried out in two steps for the parasitic elements placed at corner A. Firstly, it is done along the X-axis and then along the Y-axis (Refer to Figure 3.1).

Optimization of gap along the X axis

The process involves the shifting of a metallic strip of width 1.0 mm and length *L* along the X-axis with an increment of 0.5 mm. Initially, the strip is kept at a distance of 0.5 mm from the non-radiating edge of the antenna patch (Figure 3.2 (a)) and then the separation is gradually increased to 2.0 mm. S11 parameters for all the strips' position are simulated and studied. From the obtained results a better impedance matching is observed for a separation distance of 1.5 mm and 2.0 mm. As compactness is also one of the requirements, so a gap distance of 1.5 mm is chosen for further studies. The optimization scheme along with the corresponding S11 plots are shown in Figure 3.2.

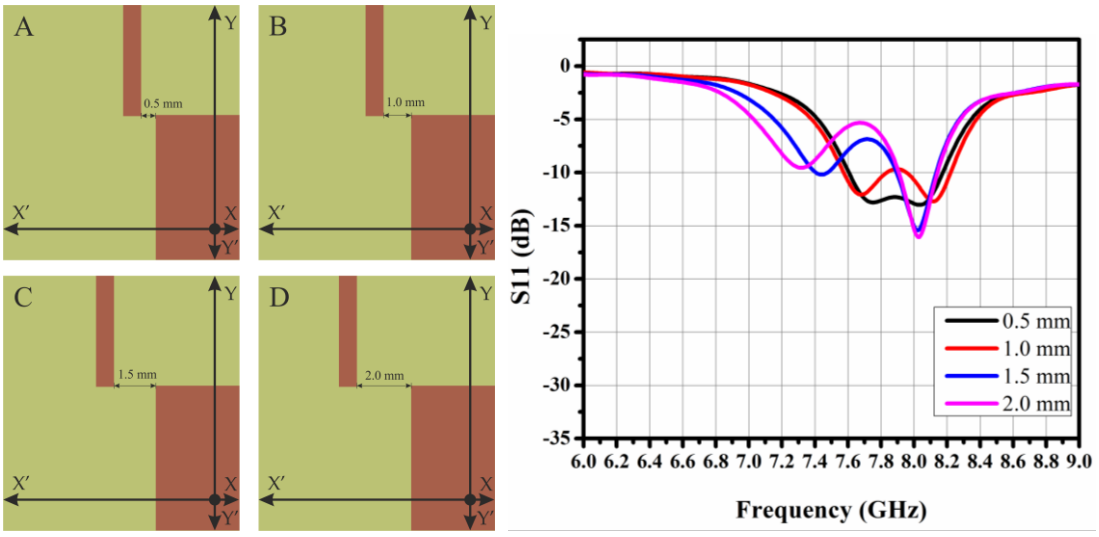

(a) (b)

Figure 3.2 (a) Representation of the gap optimization process along X axis and (b) corresponding S11 plots

Optimization of gap along the Y axis

Similar to X-axis, the position of the strip along the Y-axis is also optimized for further enhancement of the impedance matching. Here, the strip is shifted with an increment of 1.0 mm along the Y direction with reference to a starting point (Figure 3.3 (a)). S11 plots show a maximum impedance matching for a shifting distance of 1.0 mm and it is taken as the optimized position for further studies. The details of the process are shown in Figure 3.3.

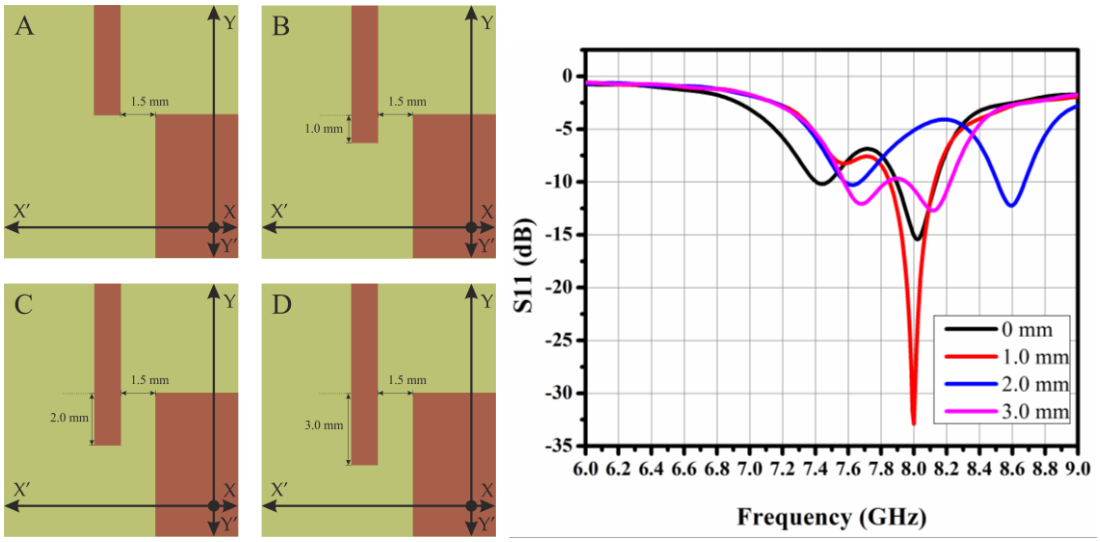

(a) (b)

Figure 3.3 (a) Representation of the gap optimization process along Y axis and (b) corresponding S11 plots

Optimization of strips numbers, width and inter strip spacing

After optimizing the strip's position in both the X and Y axis, more strips are added next to the optimized element. Four strips in parasitic elements are found to be optimum for precise controlling of the beam direction. The number can be further increased for more precision and greater beam coverage, however, to avoid system complexity it is fixed at four. (Figure 3.4). The separation distance between two consecutive elements, S_G is taken as 0.5 mm in order to ensure a good amount of mutual coupling. $S_G < 0.5$ makes the strips behave almost as a single directing (parasitic) element and shows some fabrication limitations also. Whereas, $S_G > 0.5$ reduces the coupling and hence the performance. The width of each strip is fixed at 1.0 mm to keep the overall antenna structure minimal as it is observed that there is no significant enhancement in the results with a broader strip width. Due to fabrication limitations width is not narrowed down beyond 1.0 mm. Similarly, sets located at corner B, C and D are also optimized. The details of the dimensions and positions of the antenna elements are presented in Table 3.1.

Table 3.1 Antenna design parameters

Parameter	L	W	S_L	S_G	S_W	G_S	G_T	G_B
Value (mm)	8.38	11.52	8.38	0.5	1	1.5	1	2

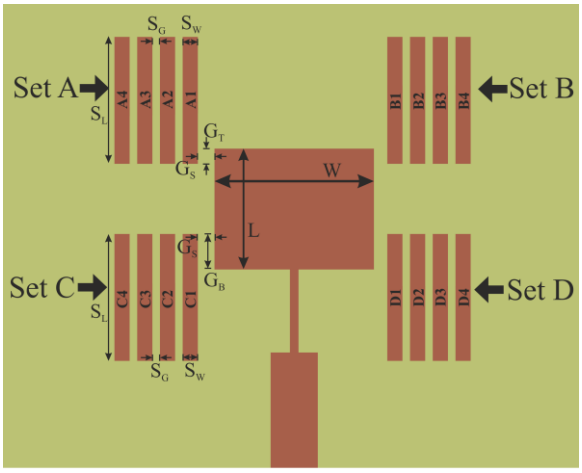

Figure 3.4 Schematic diagram of the antenna with optimized position of the elements

3.3 Reconfiguration mechanism

In order to dynamically reconfigure the beam direction a reconfiguration mechanism comprising of PIN diodes and rf inductors is used. The mechanism controls the beam direction by changing the effective length of each strip. As mentioned earlier the length of each parasitic element is crucial in Yagi formation, their beam directing behaviour is toggled through the mechanism. For this, a deliberate cut of 1mm is made at the center of each strip to insert PIN diode (BAP 72-02). Each PIN diode is separately biased by a regulated voltage of 5 V connected through a network comprising of 10 nH inductors, which acts as rf blocks.

In OFF state of the PIN diode, electrical connection between the two segments of a parasitic element is revoked and the element lacks the required length to become a director (as per Yagi formation). For this state, no modifications in the radiation pattern occur. With the activation of the PIN diode, the metallic strip acquires the necessary length and behaves as a directing element. This shifts the beam from the

broadside direction. As the antenna consists of 16 such elements, sequential activation/deactivation of the PIN diodes leads to the reconfiguration of the beam into 57 different directions. Figure 3.5 presents the schematics and fabricated antenna.

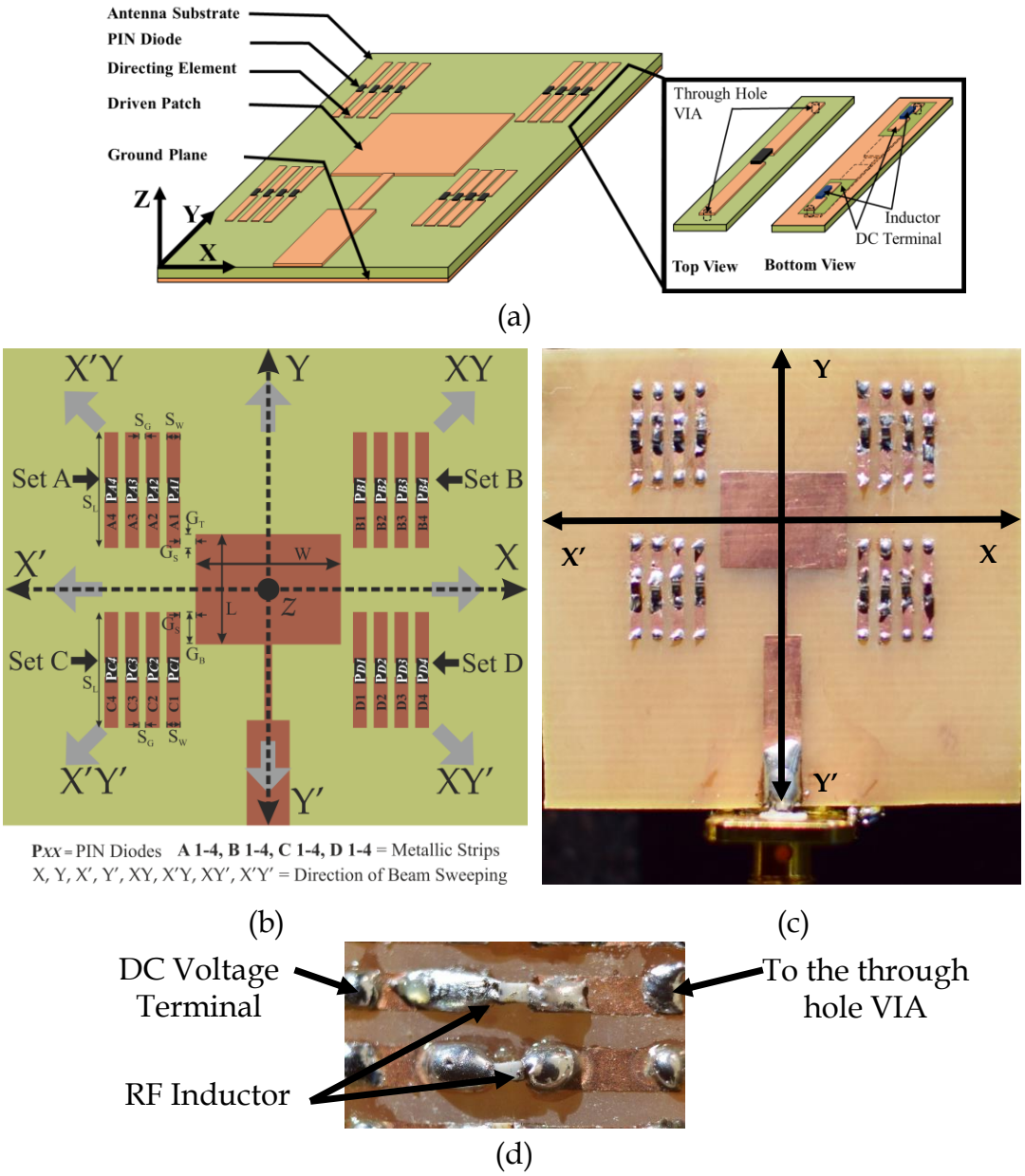

Figure 3.5 (a) Schematic diagram of the proposed antenna (b) schematic with detailed labelling of elements (c) fabricated antenna and (d) magnified view of the backside of the antenna showing the rf block inductors

3.3.1 Performance studies of beam reconfiguration

Experimental and simulation performance of the prototype antenna is carried out. First, the antenna is assessed for both return loss and radiation pattern keeping all

the PIN diodes in OFF mode. In this state, parasitic elements will not act as director (length < 0.8 L) and the antenna beam pattern is similar to that of a standard RMA, resonating at 8.0 GHz (Figure 3.6). This position is taken as reference for different beam steering angles. The antenna has a typical broadside radiation characteristics of beamwidth ~ 80˚, 0˚ beam direction, an average gain of 5 dBi and directivity nearing to 7 dB. It also exhibits a – 10 dB bandwidth of around 0.2 GHz.

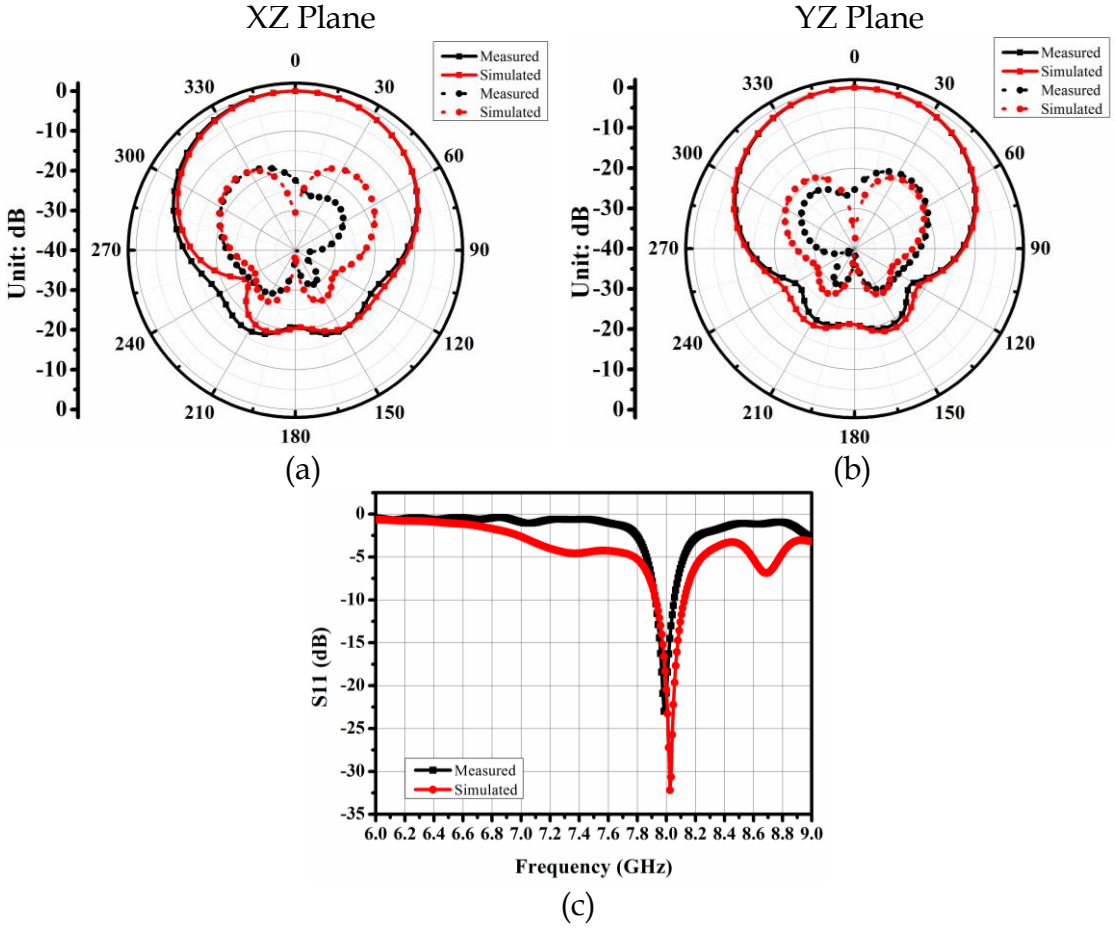

Figure 3.6 Measured and simulated -radiation patterns (a) in XZ plane (b) YZ plane (c) S11 parameters without activating any directing element

The beam is swept by controlling the state of the parasitic strips present at the four corners of the radiating patch. The sweeping is performed in two schemes-

(i) Activating strips in a single parasitic element set.

(ii) Simultaneous activation of strips in adjacent sets.

Activating strips in a single parasitic element set

The scheme activates PIN diodes attached to the metallic strips of a particular set only, while diodes of other three sets are in OFF state. The scheme is illustrated by

considering set A (Figure 3.5). PIN diodes (P_{A1} - P_{A4}) soldered to strips A1 to A4 are sequentially switched ON (Sq 1 – Sq 4) as shown in Table 3.2. The activation provides the required length for the strips to act as directing element, this deviates the beam from its initial broadside direction to X'Y direction (Figure 3.5).

Table 3.2 Reconfigured beam direction and beamwidth for Sq 0 – Sq 4

Sequence	PIN Diodes				Beam Direction XZ Plane (°)		Beam Direction YZ Plane (°)		Beamwidth XZ Plane (°)		Beamwidth YZ Plane (°)	
	A1	A2	A3	A4	Meas.	Simul.	Meas.	Simul.	Meas.	Simul.	Meas.	Simul.
Sq 0	**0**	**0**	**0**	**0**	0	0	0	0	84.97	84.98	80.00	81.08
Sq 1	**1**	**0**	**0**	**0**	355	355	10	5	92.63	86.46	74.05	72.85
Sq 2	**1**	**1**	**0**	**0**	330	340	20	15	89.88	90.98	70.65	76.58
Sq 3	**1**	**1**	**1**	**0**	320	320	30	35	90.98	88.96	73.07	74.86
Sq 4	**1**	**1**	**1**	**1**	310	315	40	40	86.64	85.48	79.08	76.88

1 = PIN Diode in ON state 0 = PIN Diode in OFF state
Meas. = Measured Simul. = Simulated

Gradual increase in the number of effective directing elements results in stepped shifting of the beam pattern. A graphical representation of the corresponding radiation pattern plots is shown in Figure 3.7. Table 3.2 also lists measured and simulated beam direction and beamwidth values of the initial condition Sq 0 in which all PIN diodes are in OFF state.

The work also includes the study of the surface current distribution for various reconfigured beam positions. As the proposed antenna design uses four sets of switchable strip lines as directing elements, the surface current study helps in understanding the working of the proposed antenna. Figure 3.8 illustrates the current distributions for sequences Sq 1 – Sq 4 and the initial Sq 0 configuration. In Sq 0 with all PIN diodes in OFF mode, there is no accumulation of current density across any of the strips and radiation pattern is the original broadside direction. As the PIN diodes are sequentially activated through Sq 1 to Sq 4, the strips turns into a director. The transformation is indicated by the build-up of current density across the strips as shown in Figure 3.8.

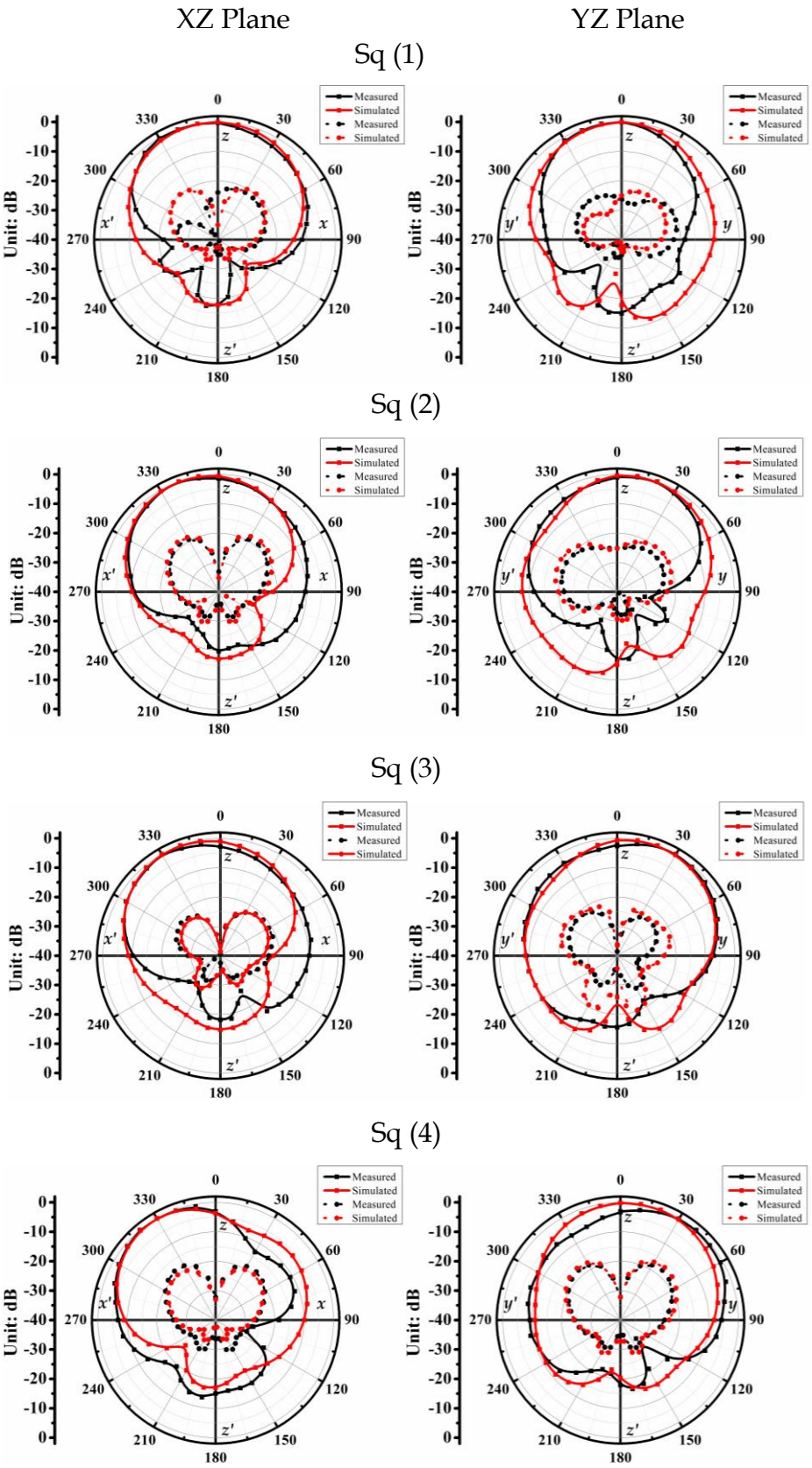

Figure 3.7 Radiation patterns in both XZ and YZ plane for sequences given in Table 3.2. Solid black and red line shows measured and simulated co-polar plots. Dotted black and red lines shows the corresponding cross-polar plots.

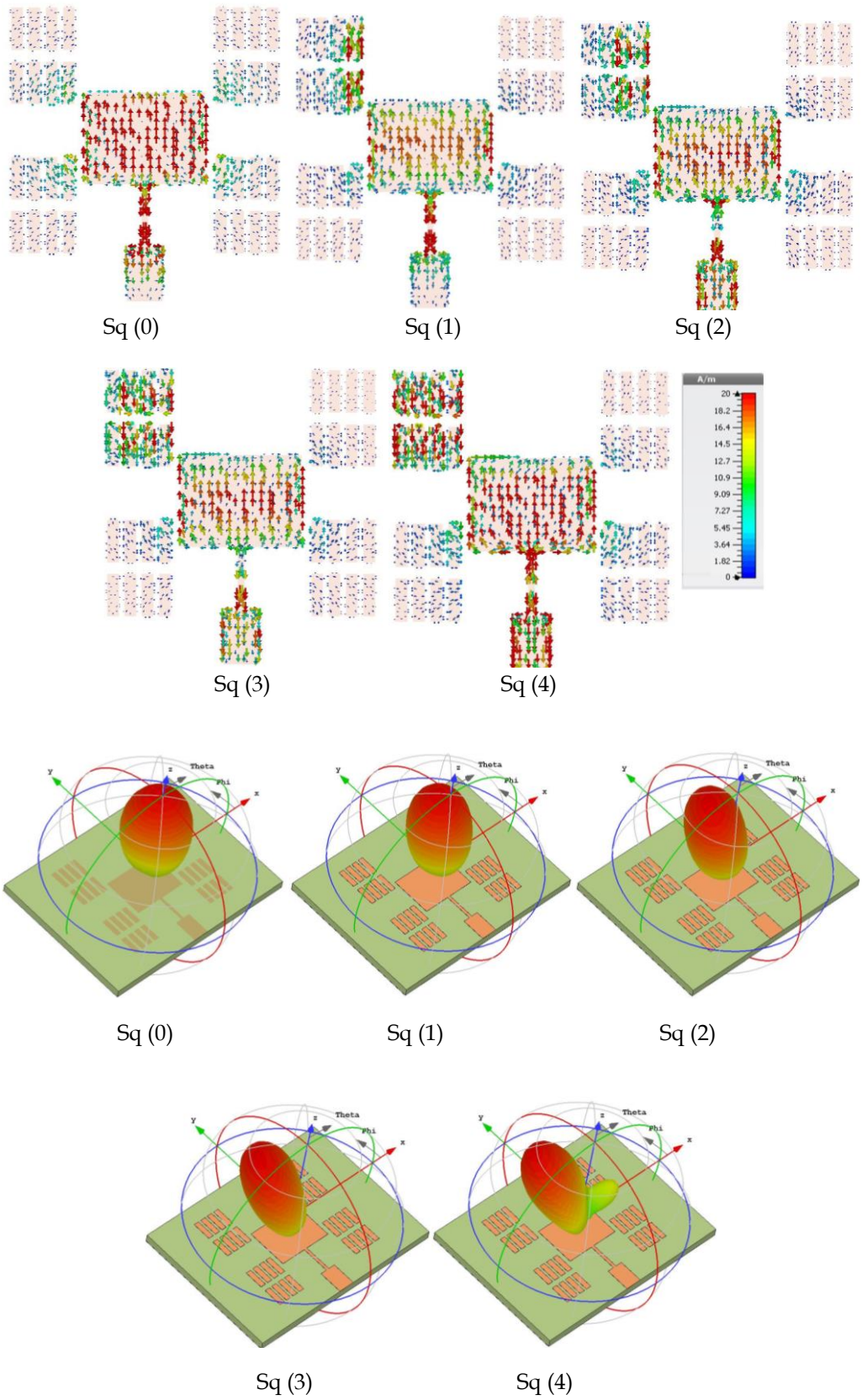

Figure 3.8 Surface current distributions and corresponding simulated radiation patterns for Table 3.2 sequences

Corresponding simulated 3 – Dimensional beam patterns are also shown in Figure 3.8. The patterns are plotted in linear scale and biasing elements are not shown in the figures as the simulation tool automatically removes them during the image extraction process. The scheme can be also applied to sets B, C and D which shifts the radiation pattern along XY, X'Y' and XY' directions respectively, in a similar way.

Simultaneous activation of strips in adjacent sets

The scheme describes combinational activations of PIN diodes in two vicinal parasitic element sets. In continuation with the previously demonstrated scheme, directing elements of sets A and C are taken for discussion. Table 3.3 lists all possible combinations of switching sequences.

Table 3.3 Combinations of PIN activation sequence from set A and C

SET C \ SET A	P_{A1} P_{A2} P_{A3} P_{A4} 1 0 0 0	P_{A1} P_{A2} P_{A3} P_{A4} 1 1 0 0	P_{A1} P_{A2} P_{A3} P_{A4} 1 1 1 0	P_{A1} P_{A2} P_{A3} P_{A4} 1 1 1 1
P_{C1} P_{C2} P_{C3} P_{C4} 1 0 0 0	$A_1 C_1$	$A_{1-2} C_1$	$A_{1-3} C_1$	$A_{1-4} C_1$
P_{C1} P_{C2} P_{C3} P_{C4} 1 1 0 0	$A_1 C_{1-2}$	$A_{1-2} C_{1-2}$	$A_{1-3} C_{1-2}$	$A_{1-4} C_{1-2}$
P_{C1} P_{C2} P_{C3} P_{C4} 1 1 1 0	$A_1 C_{1-3}$	$A_{1-2} C_{1-3}$	$A_{1-3} C_{1-3}$	$A_{1-4} C_{1-3}$
P_{C1} P_{C2} P_{C3} P_{C4} 1 1 1 1	$A_1 C_{1-4}$	$A_{1-2} C_{1-4}$	$A_{1-3} C_{1-4}$	$A_{1-4} C_{1-4}$

1 = PIN Diode in ON state 0 = PIN Diode in OFF state

In denotation, the switching sequence $A_{1-3} C_{1-2}$ (say) represents that the first three strips of the parasitic set A and first two strips of parasitic set C are active. At first, the PIN diodes in both A and C sets are switched ON, maintaining the same order and number of activated strips in both the sets. The combinations are indicated by the diagonal elements of Table 3.3. These switching sequences shift the beam in the X' direction in a stepped manner. Table 3.4 shows the simulated and measured beam directions and beamwidth of the sequences and the patterns are shown in Figure 3.9.

Table 3.4 Beam direction and beamwidth for Sq 5 – Sq 8

Sequence	PIN Diodes Combination	Beam Direction XZ Plane		Beam Direction YZ Plane		Beamwidth XZ Plane		Beamwidth YZ Plane	
		Meas.	Simul.	Meas.	Simul.	Meas.	Simul.	Meas.	Simul.
Sq 5	$A_1 C_1$	355	355	0	0	86.96	80.16	70.00	68.08
Sq 6	$A_{1-2} C_{1-2}$	330	335	0	0	82.56	81.92	66.89	68.89
Sq 7	$A_{1-3} C_{1-3}$	320	320	0	0	84.87	86.48	71.12	71.84
Sq 8	$A_{1-4} C_{1-4}$	310	315	0	0	85.64	88.46	72.28	72.18

Meas. = Measured Simul. = Simulated

Table 3.5 presents the beam statistics of the upper triangular switching sequences (Sq 9 – Sq 14) of the non-diagonal elements of Table 3.3. It is observed that for Sq 9 - Sq 14, the reconfigured patterns sweeps in between X′YZ and X′Z planes. Measured and simulated radiation pattern plots are shown in Figure 3.10.

Table 3.5 Beam direction and beamwidth for Sq 9 – Sq 14

Sequence	PIN Diodes Combinations	Beam Direction XZ Plane		Beam Direction YZ Plane		Beamwidth XZ Plane		Beamwidth YZ Plane	
		Meas.	Simul.	Meas.	Simul.	Meas.	Simul.	Meas.	Simul.
Sq 9	$A_{1-2} C_1$	330	340	30	30	88.34	88.78	72.94	73.60
Sq 10	$A_{1-3} C_1$	320	320	20	20	82.97	81.98	71.00	68.08
Sq 11	$A_{1-3} C_{1-2}$	320	320	10	5	85.47	84.14	75.44	78.52
Sq 12	$A_{1-4} C_1$	310	315	30	35	78.34	79.78	68.96	69.60
Sq 13	$A_{1-4} C_{1-2}$	310	315	20	25	82.44	80.16	66.87	65.18
Sq 14	$A_{1-4} C_{1-3}$	310	315	10	10	81.56	80.84	69.89	70.12

Meas. = Measured Simul. = Simulated

For sequencs listed in the lower triangle, the beam shifts in a similar way with the main lobe positioned in between X′Y′Z and X′Z planes. The results for these sequences are not shown in this chapter due to the similarity in nature.

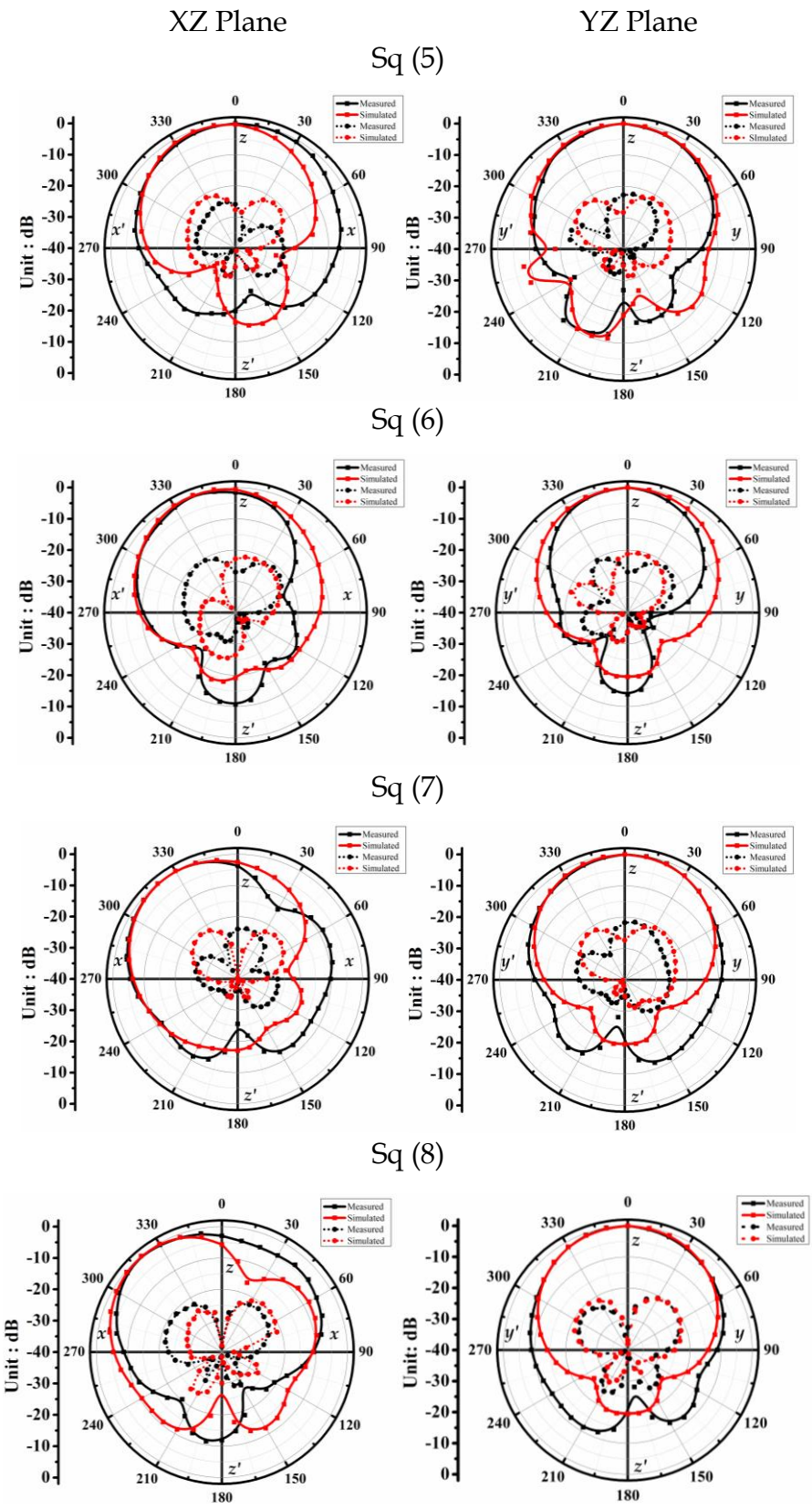

Figure 3.9 Radiation patterns in both XZ and YZ plane for sequences in given in Table 3.4. Solid black and red line shows measured and simulated co-polar plots. Dotted black and red lines shows the corresponding cross-polar plots.

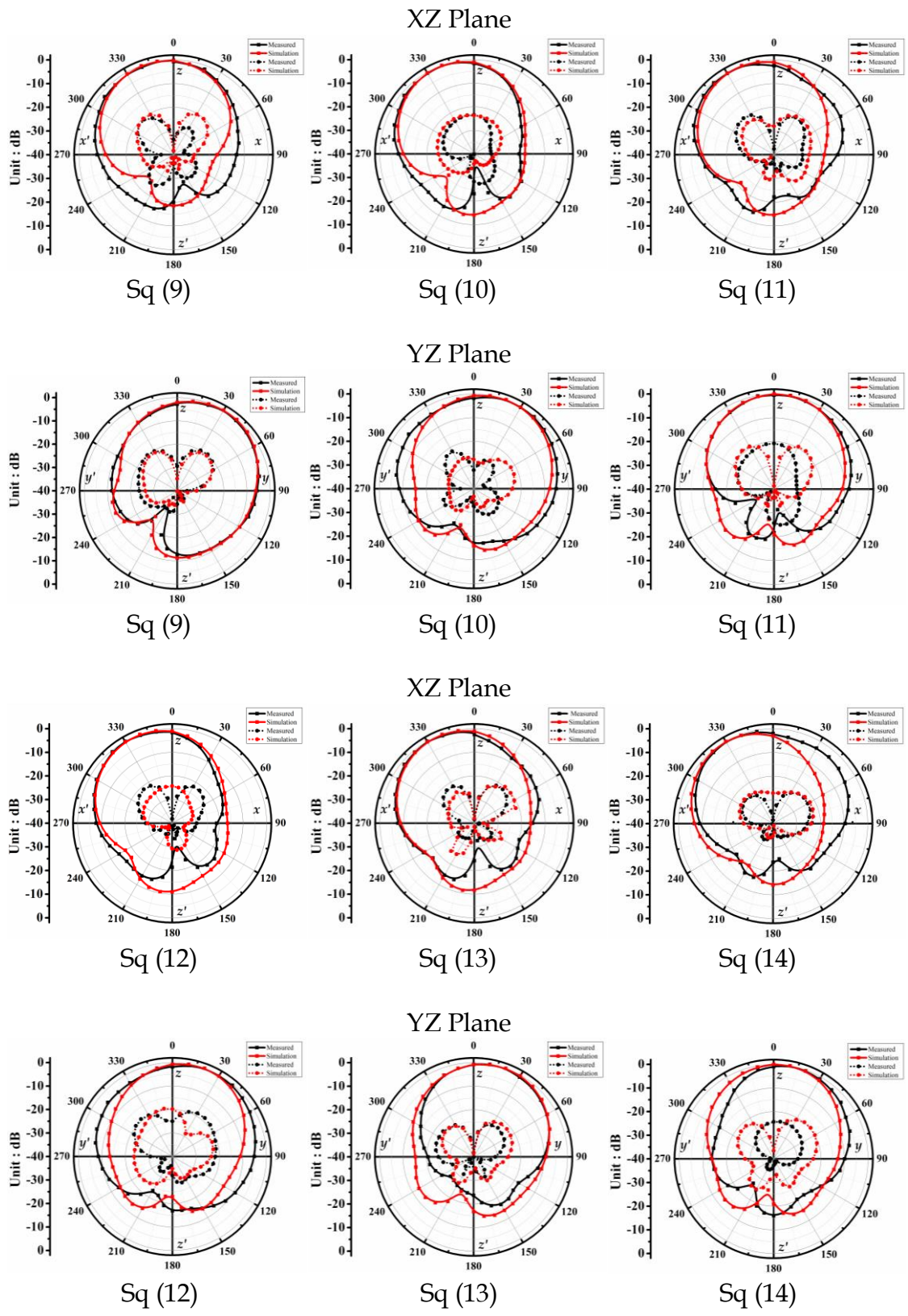

Figure 3.10 Radiation patterns in both XZ and YZ plane following sequences in Table 3.5 Solid black and red line shows measured and simulated co-polar plots. Dotted black and red lines shows the corresponding cross-polar plots.

The change in surface current distribution for these combinations are also studied and Figure 3.11 presents some of them. For the sequences, the current distribution follows the same trend as seen in Figure 3.8 and an increased current density is observed across the strips in which PIN diode is ON. Figure 3.11 also shows 3 - Dimensional beam patterns of the sequences.

The antenna is also tested for the consistency in terms of its operating frequency, directivity, gain and efficiency. A tabulated comparison of these parameters for the sequences Sq 0– Sq 14 is given in Table 3.6. The measured results show that the antenna can redirect the beam towards the directions discussed without much variation in the resonant frequency range ($\Delta f \cong \pm 0.1$ GHz). Directivity, gain and efficiency are also fairly stable in all the directions as observed in Table 3.6.

Table 3.6 Measured antenna parameters for sequences Sq 0 – Sq 14

Sequence	Frequency (GHz)	Bandwidth (-10 dB) (MHz)	Directivity (dB)	Gain (dBi)	Efficiency
Sq 0	8.00	200	6.0	5	83%
Sq 1	8.08	180	6.0	5	83%
Sq 2	7.86	200	6.4	4.8	75%
Sq 3	7.92	196	6.2	4.4	71%
Sq 4	7.98	192	6.0	4.2	70%
Sq 5	7.86	184	6.8	5.2	76%
Sq 6	7.82	206	7.5	4.9	65%
Sq 7	7.92	198	7.2	4.6	64%
Sq 8	7.94	194	7.1	4.9	69%
Sq 9	7.98	190	6.4	4.8	75%
Sq 10	8.06	196	7.0	4.9	70%
Sq 11	8.02	204	6.4	4.7	73%
Sq 12	8.00	208	7.6	4.9	64%
Sq 13	7.94	200	7.4	4.8	65%
Sq 14	7.96	198	7.2	4.9	68%

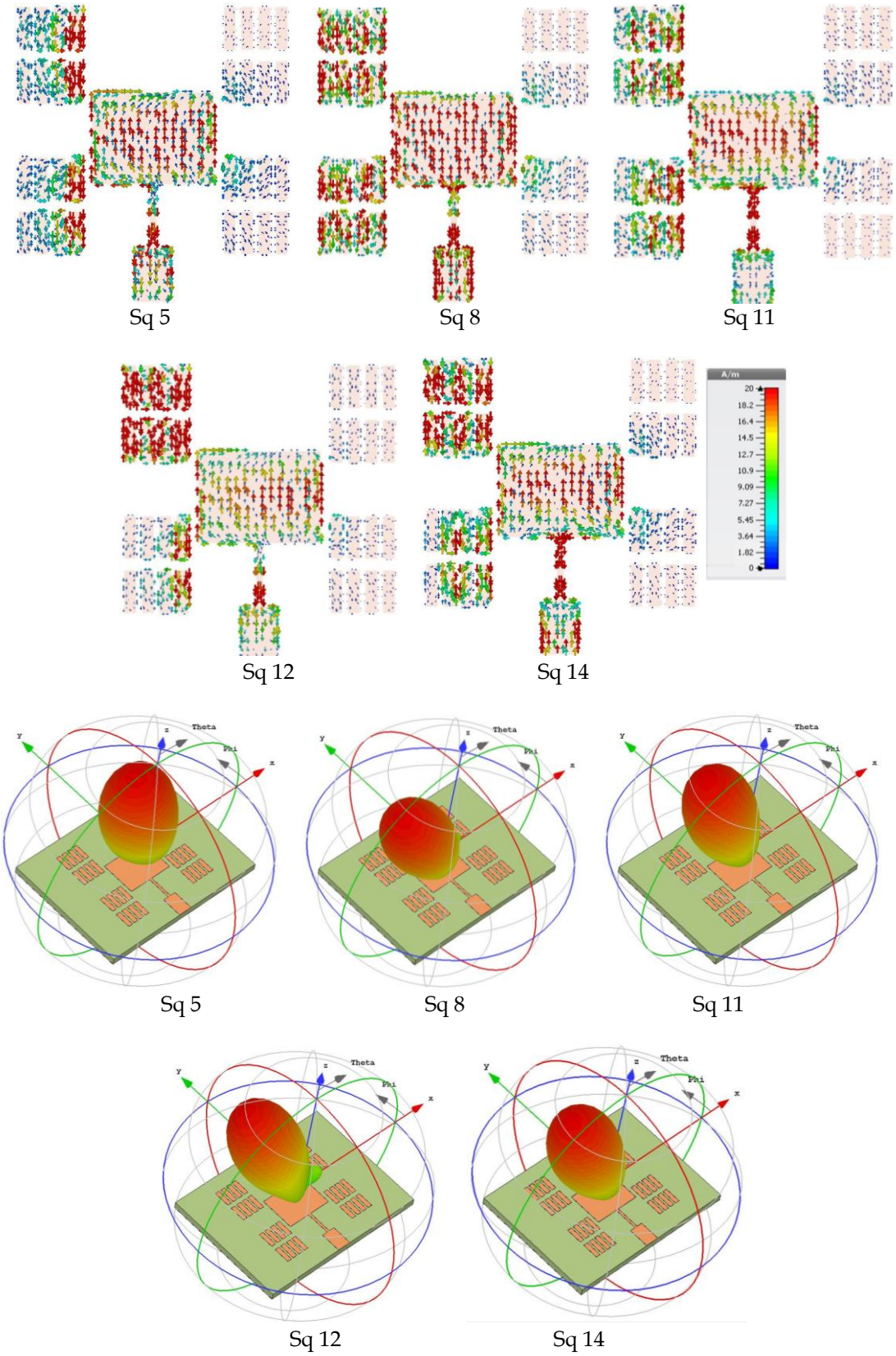

Figure 3.11 Surface current distribution and corresponding simulated radiation patterns

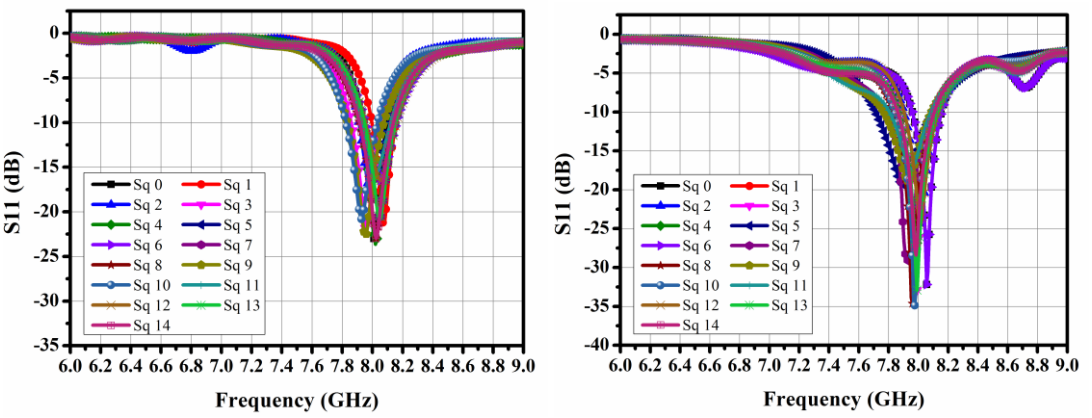

Figure 3.12 (a) Measured and (b) simulated S11 plots for sequences Sq 0 – Sq 14

Figure 3.12 shows the measured and simulated S11 parameters of the antenna for sequences Sq 0 – Sq 14.

Beam pattern of the proposed antenna for remaining possible sequences

Studies are also conducted to verify the antenna performances for other activation sequences involving parasitic elements of set B, C and D. However, the enormous data and combinations have restricted in putting the data in this chapter. Since the results are akin to the set A-C studied, except for the direction of beam steering, only some of the combinations are presented in Table 3.7.

Table 3.7 Beam pattern statistics for some of the selected combinations

Activated Set	Frequency (GHz)	Main Lobe Direction (°)				Beamwidth (°)			
		Measured		Simulated		Measured		Simulated	
		XZ Plane	YZ Plane	XZ Plane	YZ Plane	XZ Plane	YZ Plane	XZ Plane	YZ Plane
B_{1-4}	7.94	40	320	30	330	95.17	67.00	75.58	63.76
C_{1-4}	7.98	310	40	320	30	62.26	62.06	77.72	88.30
D_{1-4}	7.96	40	30	40	30	70.74	62.00	88.14	70.02
AB_{1-4}	7.96	0	320	0	330	65.24	80.02	103.70	63.92
DC_{1-4}	7.94	0	40	0	30	99.00	75.44	67.27	63.12
BD_{1-4}	8.00	40	0	40	0	95.34	64.94	88.78	65.60

In the Table 3.7 beam directions with the maximum obtained shifts are listed. For this, all the PIN diodes in one single set or more are activated. For example, listing

for activated set B shows the beam pattern characteristics with all the PIN diodes in set B are in ON state and so on. The results are in accordance with the observations presented for the sets A and C. This validates the idea to cover a spherical distribution with an apex angle of ~ 80˚ (± 40˚) normal to the plane of the antenna patch. Figure 3.13 shows the corresponding simulated 3 – Dimensional radiation patterns.

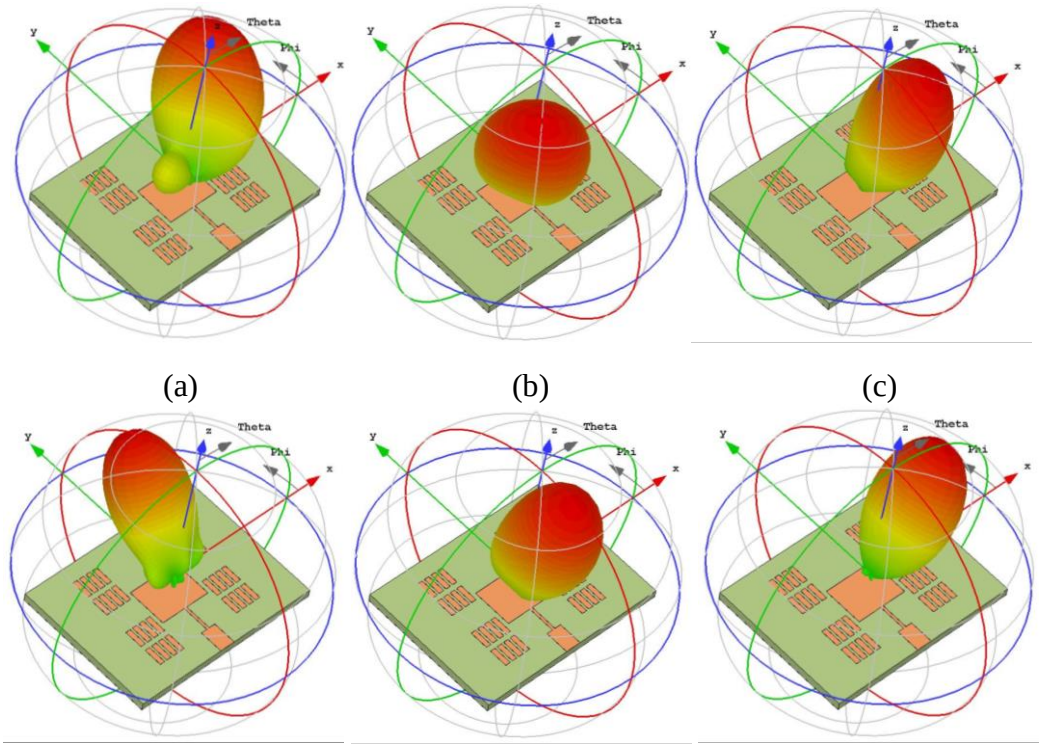

Figure 3.13 Simulated 3-D radiation patterns for activated set (a) B, (b) C, (c) D, (d) AB, (e) DC and (f) BD

3.4 Discussion

The proposed pattern reconfigurable antenna can alter the beam up to 57 directions. The beam can be tilted up to ~ 40˚ off broadside and can sweep the entire azimuth plane. For the sequence Sq 1 – Sq 4 the beam sweeps in X'Y direction with main lobe directions (355˚, 10˚), (330˚, 20˚), (320˚, 30˚) and (310˚, 40˚) respectively. A gradually tilted beam in X' direction with beam angles (355˚, 0˚), (330˚, 0˚), (320˚, 0˚) and (310˚, 0˚) is observed for Sq 5 – Sq 6. The antenna pattern is

positioned at (330˚, 30˚), (320˚, 20˚), (320˚, 10˚), (310˚, 30˚), (310˚, 20˚) and (310˚, 10˚) for sequence Sq 9 – Sq 14.

The prototype antenna is also tested for stability of the operating frequency while reconfiguring the beam pattern. The resonating frequency is at around 8.00 GHz for all the sequences (Sq 0 – Sq 14), which is fairly constant. The directivity and gain are also consistent and are in the range of 7.6 dB – 6.0 dB and 5.2 dB – 4.2 dB respectively. The antenna has a low profile structure and offers relatively high numbers of beam sweeping angle. A comparison of some of the recent reconfigurable antenna is presented in Table 3.8 and it is observed that the proposed antenna has the highest number of switchable beam directions.

Table 3.8 Comparison of the proposed antenna with previously reported recent works of pattern reconfigurable antenna

Ref. No.	Antenna Geometry	Frequency (GHz)	Frequency Stability	No. of Switchable Beam	Plane of Reconfiguration	Peak Gain (dBi)
[5]	Planar	2.08	Yes	4	Dual, E and H	4.58
[13]	Planar	2.40	Yes	9	Dual, Azimuthal and Elevation	7.00
[19]	Planar	5.80	Yes	3	Dual	5.00
[20]	Non – Planar	2.45	Yes	5	Single, Elevation	6.50
[21]	Planar	2.40	Yes	4	Single, Azimuthal	3.70
Proposed	Planar	8.00	Yes	57	Dual, Azimuthal and Elevation	5.00

The proposed method for sequential activation or deactivation of the directing elements is also verified by the surface current distribution studies. The accumulation of current across the electrically connected strips indicate the mutual coupling between the antenna patch and the directors resulting in the beam tilt. The reduced current density across the electrically disconnected strips marks the absence of mutual coupling.

The segmented design of parasitic elements helps in sweeping the beam in multiple steps. Thus, enabling the antenna to scan a spherical distribution with an apex angle of ~ 80˚ in the broadside direction of the patch.

References

[1] Ding, X., and Wang, B.Z. A Novel Wideband Antenna With Reconfigurable Broadside and Endfire Patterns. *IEEE Antennas and Wireless Propagation Letters,* 12:995-998, 2013. DOI:10.1109/LAWP.2013.2278139

[2] Huff, G.H., Feng, J., Zhang, S., and Bernhard, J.T. A novel radiation pattern and frequency reconfigurable single turn square spiral microstrip antenna. *IEEE Microwave and Wireless Components Letters,* 13(2):57-59, 2003. DOI:10.1109/LMWC.2003.808714

[3] Wang, B.Z., Xiao, S., Bai, Y.Y., and Zhang, G.M. Researches on pattern reconfigurable antenna and its application in phased array. in *2011 International Workshop on Antenna Technology (iWAT)*, 46-49, 2011.

[4] Wu, W., Wang, B.-Z., Yang, X.-S., and Zhang, Y. A pattern-reconfigurable planar fractal antenna and its characteristic-mode analysis. *IEEE antennas and propagation magazine,* 49(3):68-75, 2007.

[5] Nair, S.V.S., and Ammann, M.J. Reconfigurable Antenna With Elevation and Azimuth Beam Switching. *IEEE Antennas and Wireless Propagation Letters,* 9:367-370, 2010. DOI:10.1109/LAWP.2010.2049332

[6] Riel, M., and Laurin, J.J. Design of an Electronically Beam Scanning Reflectarray Using Aperture-Coupled Elements. *IEEE Transactions on Antennas and Propagation,* 55(5):1260-1266, 2007. DOI:10.1109/TAP.2007.895586

[7] Sievenpiper, D., Schaffner, J., Loo, R., Tangonan, G., Ontiveros, S., and Harold, R. A tunable impedance surface performing as a reconfigurable beam steering reflector. *IEEE Transactions on Antennas and Propagation,* 50(3):384-390, 2002. DOI:10.1109/8.999631

[8] Preston, S., Thiel, D., Lu, J.W., O'keefe, S., and Bird, T. Electronic beam steering using switched parasitic patch elements. *Electronics Letters,* 33(1):7-8, 1997.

[9] Jusoh, M., Sabapathy, T., Jamlos, M.F., and Kamarudin, M.R. Reconfigurable four-parasitic-elements patch antenna for high-gain beam switching application. *IEEE Antennas and Wireless Propagation Letters,* 13:79-82, 2014.

[10] Cai, Y., and Du, Z. A Novel Pattern Reconfigurable Antenna Array for Diversity Systems. *IEEE Antennas and Wireless Propagation Letters,* 8:1227-1230, 2009. DOI:10.1109/LAWP.2009.2035720

[11] Eslami, H., Sukumar, C.P., Rodrigo, D., Mopidevi, S., Eltawil, A.M., Jofre, L., and Cetiner, B.A. Reduced Overhead Training for Multi Reconfigurable Antennas with Beam-Tilting Capability. *IEEE Transactions on Wireless Communications,* 9(12):3810-3821, 2010. DOI:10.1109/TWC.2010.091510.100267

[12] Donelli, M., Azaro, R., Fimognari, L., and Massa, A. A Planar Electronically Reconfigurable Wi-Fi Band Antenna Based on a Parasitic Microstrip Structure. *IEEE Antennas and Wireless Propagation Letters,* 6:623-626, 2007. DOI:10.1109/LAWP.2007.913274

[13] Jusoh, M., Aboufoul, T., Sabapathy, T., Alomainy, A., and Kamarudin, M.R. Pattern-Reconfigurable Microstrip Patch Antenna With Multidirectional Beam for WiMAX Application. *IEEE Antennas and Wireless Propagation Letters,* 13:860-863, 2014. DOI:10.1109/LAWP.2014.2320818

[14] Yang, X.S., Wang, B.Z., Wu, W., and Xiao, S. Yagi Patch Antenna With Dual-Band and Pattern Reconfigurable Characteristics. *IEEE Antennas and Wireless Propagation Letters,* 6:168-171, 2007. DOI:10.1109/LAWP.2007.895292

[15] Sharma, S.K., Fideles, F., and Kalikonda, A. Radiation pattern reconfigurable planar Yagi-Uda antenna. in *2013 IEEE Antennas and Propagation Society International Symposium (APSURSI)*, 190-191, 2013.

[16] Zhang, S., Huff, G.H., Feng, J., and Bernhard, J.T. A pattern reconfigurable microstrip parasitic array. *IEEE Transactions on Antennas and Propagation,* 52(10):2773-2776, 2004. DOI:10.1109/TAP.2004.834372

[17] Balanis, C.A. *Antenna theory: analysis and design.* John Wiley & Sons. 2016.

[18] Huang, J., and Densmore, A.C. Microstrip Yagi array antenna for mobile satellite vehicle application. *IEEE Transactions on Antennas and Propagation,* 39(7):1024-1030, 1991. DOI:10.1109/8.86924

[19] Wang, R., Wang, B., Gao, G., Ding, X., and Wang, Z. Low-Profile Pattern-Reconfigurable Vertically Polarized Endfire Antenna With Magnetic-Current Radiators. *IEEE Antennas and Wireless Propagation Letters,* 17(5):829-832, 2018. DOI:10.1109/LAWP.2018.2817682

[20] Chen, S., Qin, P., Lin, W., and Guo, Y.J. Pattern-Reconfigurable Antenna With Five Switchable Beams in Elevation Plane. *IEEE Antennas and Wireless Propagation Letters,* 17(3):454-457, 2018. DOI:10.1109/LAWP.2018.2794990

[21] Alam, M.S., and Abbosh, A.M. Wideband Pattern-Reconfigurable Antenna Using Pair of Radial Radiators on Truncated Ground With Switchable Director and Reflector. *IEEE Antennas and Wireless Propagation Letters,* 16:24-28, 2017. DOI:10.1109/LAWP.2016.2552492